J. Fluid Mech. (2012), *vol.* 702, *pp.* 354–377.
doi:10.1017/jfm.2012.182

Spatial modes of capillary jets, with application to surface stimulation

J. Guerrero[1,3], H. González[1,3]† and F. J. García[2,3]

[1] Departamento de Física Aplicada III, Escuela Técnica Superior de Ingenieros, Universidad de Sevilla, Camino de los Descubrimientos, s/n 41092-Sevilla, Spain

[2] Departamento de Física Aplicada I, Escuela Técnica Superior de Ingeniería Informática, Universidad de Sevilla, Avenida Reina Mercedes, s/n. 41012-Sevilla, Spain

[3] Group of Electrohydrodynamics and Cohesive Granular Media, Facultad de Física, Universidad de Sevilla, Avenida Reina Mercedes, s/n. 41012-Sevilla, Spain

(Received 29 April 2011; revised 13 February 2012; accepted 12 April 2012; first published online 16 May 2012)

Surface stimulation of any physical origin (electrohydrodynamic, thermocapillary, etc.) has the goal of generating localized perturbations on the free surface or the velocity field of a capillary jet. Among these perturbations, only the axisymmetric ones are determinant for the jet breakup. Often, the stimulation is weak enough for a linear model to be applicable. Then, the stimulation can be described by means of the Green functions for stresses, both normal and tangential to the interface, the calculations of which are, in addition, uncoupled from the hydrodynamic variables. If a harmonic forcing is applied, these Green functions are combinations of the spatial modes whose associated poles lie inside the appropriate integration contour of the complex wavenumber plane. This is the motivation for a comprehensive enumeration and description of the spatial modes, which has not been done up to now. Modes familiar from a temporal analysis, the dominant and subdominant capillary modes and the hydrodynamic modes, are present, along with modes specific to a spatial analysis. Most of the latter have already been mentioned in the literature for inviscid jets, but not analysed. A mode not previously found is reported. In addition, a description of the velocity field associated with each mode is provided, as a tool to understand their physical origin and behaviour. The relative importance of each mode in both normal- and tangential-stress stimulations is discussed. Finally, the well-known merging of poles below a critical jet velocity, leading to absolute instability, is analysed in the light of the modal description.

Key words: capillary flows, waves/free-surface flows

1. Introduction

The stimulation of capillary jets issuing from a nozzle for controlled production of drops is nowadays widely applied in many industrial and technological processes, such as ink-jet printing, microfluidics, combinatorial chemistry, biological assays, combustion science and aerosol science. For a perspective of the relevance and

† Email address for correspondence: helio@us.es

variety of stimulation techniques the reader can consult the work of Lee (2003). For our purpose, we can classify all these techniques in two groups: stimulation at the nozzle and surface stimulation. By stimulation at the nozzle we mean devices acting on any part of the reservoir of the liquid to be ejected, i.e. piezoelectric and bubble-jet setups. On the other hand, by surface stimulation we mean any stimulation mechanism acting on the surface of the jet once it has been formed. Consequently, it is, in general, independent of the reservoir and nozzle features, especially if the stimulation region is at a distance for which the initial velocity profile has relaxed to a uniform one. At the same time, this distance has to be short enough in order that the amplitude of stimulation is significantly greater than the noise-induced amplitude of the most rapidly growing mode. The independence of nozzle and stimulation is the main advantage of these devices, as it makes possible multi-jet assemblies stimulated without acoustic coupling between the individual jets. Electrohydrodynamic (EHD) and thermocapillary stimulations are the best-known implementations of this kind of stimulation.

In EHD stimulation (Goedde & Yuen 1970; Crowley 1983; Barbet 1997), an electric field is usually set by means of an electrode placed very close to the jet surface, not too far from the nozzle. Shielding by other grounded electrodes is convenient (González & García 2009) to keep the region of electrostatic influence on the jet narrow. In this way, an electric stress is applied over that region. For perfect conductors, we only have a normal electrostatic stress, but for finite electrical conductivity we also have a modest tangential stress as the jet is no longer equipotential.

In thermocapillary stimulation (Nahas & Panton 1990; Barbet 1997), a laser beam with modulated intensity heats the surface of the jet, yielding a spatial distribution of temperature on it. As the surface tension depends on the temperature, we have two physical effects: (i) a decrease of capillary pressure in the hot region, where the surface tension is lower; and (ii) a Marangoni tangential stress, given by the gradient of the surface tension. We refer the reader to the work of Barbet (1997) where, in the chapter devoted to the thermal stimulation, we can find estimates of the relative importance of pressure and tangential-stress contributions, and the typical length at which the temperature gradients persist on the jet surface. Under his experimental conditions, he concluded that the stimulation due to the Marangoni effect is one order of magnitude stronger than that arising from the differences in capillary pressure, and that the rise in surface temperature is restricted to a short length (one to five times the jet diameter).

A common feature of these two surface stimulations is the low amplitude of deformation achieved after the stimulation, compared with those obtainable by nozzle stimulation. As an example, EHD stimulation of submillimetric jets typically produces initial perturbations of the order of 10^{-3} times the jet radius, to be compared with a typical noise level of 10^{-5} (Barbet 1997); electric breakdown limits that initial perturbation factor to 10^{-2} in experiments reported in González & García (2009). Furthermore, these perturbations yield an impulse rather than a deformation. The main consequence is that the jet can be considered as virtually cylindrical over the whole stimulation region, provided that it remains reasonably local (by using the above-mentioned shielding electrodes in one case or having a sufficiently high thermal conductivity in the other). This enables us to apply two important simplifications from a mathematical point of view (Crowley 1983, 1986; Spohn & Atten 1993):

(i) the stimulation problem is linear; and (ii) the stresses can be calculated under the assumption that the jet is a cylinder, so they are uncoupled from the hydrodynamic variables. Strong or very extended stimulations, which are not the usual cases, will be disregarded.

As the problem is linear and the surface stresses are inputs independent of the hydrodynamic variables, the Green function formalism is the best approach. Specifically, we are interested in the Green function for an infinite jet with uniform velocity profile, with the surface stresses as the inhomogeneous terms. This provides a useful tool to characterize either EHD, thermocapillary or any kind of surface stimulation. In doing so, we will find expressions where the spatial modes are superposed. This is the motivation for a systematic characterization of the modes, prior to the understanding of the Green function itself.

In spite of the impressive number of works (Eggers 1997; Lin 2003; Eggers & Villermaux 2008) published on capillary jets since the pioneering research of Plateau (1873) and Rayleigh (1945), the modal analysis of the basic model is not still complete. This is perhaps due to the success in the description of the instability by means of merely considering the only mode which is unstable, for wavelengths greater than $2\pi R$ (R is the unperturbed radius of the jet). This analysis has been recently carried out from a temporal-instability point of view in García & González (2008). There, as Lord Rayleigh proposed, the unperturbed jet is considered to be an infinitely long column at rest. The authors state that, in addition to the two well-known capillary modes, one being the previously mentioned unstable mode, there called the *dominant capillary mode*, and the other that is always stable, called the *subdominant capillary mode*, there exists an infinite number of decaying modes, the *hydrodynamic modes*. Capillary modes are originated by competition between capillary forces and inertia (and eventually viscosity); they have a significant free-surface deformation and their combination is sufficient to describe any perturbation in both the jet shape and the mean axial velocity. On the other hand, hydrodynamic modes have their origin in a balance between inertia and viscous forces, and are essentially described as having recirculating velocity flows and small surface deformations. They have been previously described in liquid bridges (Nicolás & Vega 2000) but ignored in jets. The two capillary modes and the hydrodynamic family form a complete basis for any axisymmetric perturbation of the infinite viscous jet.

Since the work of Keller, Rubinow & Tu (1973) on inviscid capillary jets, the temporal approach has been viewed as the limit for large jet velocities of the more realistic description provided by the spatial analysis, for which the jet exits from a nozzle and perturbations are allowed to evolve spatially. In addition to two spatial modes related to the temporal capillary modes, Keller and co-workers found another family, infinitely numerous, with striking features: growth much greater than the dominant capillary mode and very long wavelength. They are specific to the spatial analysis, with no counterpart in the temporal analysis. There is little description of these modes in Keller's article, as their behaviour was considered rather unphysical. Based on their long wavelength, they were discarded as not observable in experiments. Alternatively, Bogy (1978) gave radiation arguments to make the same conclusion. Also, there was another inviscid mode mentioned by Busker & Lamers (1989) and not found by Keller and co-workers, which was originally reported by Boersma (private communication). However, all we knew about this mode was its mere existence and its asymptotic location in the complex wavenumber plane (hereafter referred to as

the k-plane) for large jet velocities. More recently, the same mode was taken into account in the search for global modes of falling capillary jets by Le Dizès (1997). Finally, a new mode with similar origin as Boersma's mode, not reported up to now, must be added to the list, as we shall show.

Not long after Keller's work, the concepts of convective and absolute instabilities (Briggs 1964; Bers 1983; Huerre & Monkewitz 1990) were applied to the capillary jet by Leib & Goldstein (1986*a*). In this first article, the authors considered inviscid liquids and a Hagen–Poiseuille velocity profile, including the plug profile as a limit. The detection of the existence of absolute instability, i.e. amplifying waves in the whole jet, does not need a complete description of the spatial modes arising from the dispersion relation. They only had to show the merging of two of these modes coming from different half-planes in the complex k-plane as the imaginary part of their complex frequency goes to zero. As a consequence, the characterization of the whole set of modes was not addressed in that work. The same happened in later extensions to viscous capillary jets (Leib & Goldstein 1986*b*). The task of determining and describing the spatial modes has been systematically omitted.

In general, the location in the complex k-plane of the zeros and branch cuts of a dispersion relation corresponding to any physical system does not give all the relevant information about stability. The dispersion relation arises in a natural way as the denominator of the spatio-temporal Fourier transform of the Green function for any specific boundary conditions. The Green function is obtained by means of the inversion formula with appropriate Bromwich paths in the complex ω- and k-planes satisfying causality conditions (Briggs 1964). It is necessary to monitor the movement of these zeros as we let the imaginary part of the complex frequency go to zero. This procedure defines a clear separation of the zeros (poles of the transform of the Green function) into two sets affecting the flow upstream and downstream, respectively. Only then do the poles reveal the growing or decaying nature of their associated modes (in Gordillo & Pérez-Saborid 2002 we can find an alternative procedure for this mode-assignment task). The perplexity generated by the unphysical solutions in Keller's work is due to his analysis being limited to the dispersion relation, without consideration of the complete physical problem.

The problem formulation and formal solutions for the spatial Green functions of surface stimulation, for both normal and tangential stresses, are presented in the next section. By spatial Green functions we mean those arising when we assume the same harmonic temporal dependence as the stimulation stresses. In § 3 we classify and describe the location of poles and their associated velocity field for the full set of spatial modes involved in the general solution previously obtained. Section 4 analyses the two Green functions in terms of their modal structure. With a practical purpose, their stimulation performances are compared. Section 5 pays particular attention to the generation of absolute instability from two specific spatial modes, not always well-determined in previous works (Yakubenko 1997). In § 6, we discuss several consequences: the physical interpretation of each mode, their relative participation in both kinds of stimulation, their role in the generation of absolute instability, the relation of some modes to the phenomenon of static corrugations observed upstream of a jet impinging on an obstacle or fluid surface (Awati & Howes 1996; Hancock & Bush 2002) and, finally, practical consequences regarding stimulation.

2. Problem formulation

Consider a jet infinitely extended both upstream and downstream from a stimulation zone, made of a viscous liquid, with unperturbed radius R and uniform axial velocity v_0. The liquid has density ρ, dynamic viscosity μ and surface tension γ. The outer medium is a gas and it is assumed to have negligible dynamics, a realistic assumption for not too large relative velocities between the jet and the outer medium (Gordillo & Pérez-Saborid 2005; González & García 2009).

The dynamics of the jet is governed by the Navier–Stokes equations for incompressible fluids, with no bulk forces (gravity is neglected). In terms of small perturbations with respect to the basic flow we can write in dimensionless form:

$$\boldsymbol{\nabla}\cdot\boldsymbol{v}=0, \tag{2.1}$$

$$\left(\frac{\partial}{\partial t}+\beta\frac{\partial}{\partial z}\right)\boldsymbol{v}=-\boldsymbol{\nabla}p+C\nabla^2\boldsymbol{v}, \tag{2.2}$$

where we define, using cylindrical coordinates, the axisymmetrically perturbed velocity field $\boldsymbol{v}(r,z,t)=u(r,z,t)\,\boldsymbol{e}_r+w(r,z,t)\,\boldsymbol{e}_z$ ($\boldsymbol{e}_r$ and $\boldsymbol{e}_z$ being the radial and axial unit vectors) and the perturbed pressure field $p(r,z,t)$. Here we have scaled lengths with R, time with $t_c\equiv(\rho R^3/\gamma)^{1/2}$ (capillary time), velocity with R/t_c and pressure with γ/R. Two non-dimensional numbers arise: the non-dimensional jet velocity, $\beta=v_0\,(\rho R/\gamma)^{1/2}$ (hereafter called *jet velocity*), and the Ohnesorge number, $C=\mu/\,(\gamma\rho R)^{1/2}$.

Let us describe the jet shape by the equation $r=1+f(z,t)$, where $f(z,t)$ will be called the surface deformation. The boundary conditions at the free surface are the kinematic condition and the normal and tangential stress balances. In linearized form these are, respectively,

$$\frac{\partial f}{\partial t}+\beta\frac{\partial f}{\partial z}-u=0, \tag{2.3}$$

$$-f-\frac{\partial^2 f}{\partial z^2}-p+2C\frac{\partial u}{\partial r}=T_n, \tag{2.4}$$

$$C\left(\frac{\partial u}{\partial z}+\frac{\partial w}{\partial r}\right)=T_t, \tag{2.5}$$

where all magnitudes are evaluated at $r=1$. Here we need to define the normal, T_n, and tangential, T_t, stresses, of any origin (electric, magnetic, thermocapillary), acting on the free surface. Stresses are consistently scaled with γ/R and their signs are defined in accordance with the positive direction of the radial and axial coordinates. In what follows, we shall assume that the stresses are inputs uncoupled from the hydrodynamic problem. As an example, in EHD stimulation both kinds of stresses can be calculated from the Maxwell stress tensor by independently solving the quasi-electrostatic problem defined by the jet, assumed cylindrical, and the external electrodes.

The adopted non-dimensionalization, based on capillary forces, is not the usual one found in the literature based on advective inertia that introduces the Weber number, $We\equiv\beta^2$, and the Reynolds number, $Re\equiv\rho v_0 R/\mu$, instead of the Ohnesorge number, the relation being $C=\beta/Re$. The main advantage of our choice is to have only one control parameter, β, in experiments. Also, capillary forces are the best reference to measure forces and external stresses, as inertia is related more to the wavelength selection of perturbations than to their amplitudes. In fact, this is the reason for the

success of the temporal approach, to which the spatial analysis is related in the most natural way as the limit $\beta \gg 1$.

We are interested in harmonic stimulation, so we consider a temporal harmonic dependence for the two stresses $T_n(z)\exp(\mathrm{i}\omega t)$ and $T_t(z)\exp(\mathrm{i}\omega t)$, where ω is the imposed non-dimensional angular frequency (we have maintained the symbols T_n and T_t as functions of z alone because there is no ambiguity). Let us assume for the function $\boldsymbol{Q}(r,z,t) \equiv \{p(r,z,t), u(r,z,t), w(r,z,t), f(z,t)\}$,

$$\boldsymbol{Q}(r,z,t) = \mathrm{Re}[\boldsymbol{q}(r,z)\exp(\mathrm{i}\omega t)], \tag{2.6}$$

with $\boldsymbol{q}$ a complex function, and define the Fourier transform in the axial variable as

$$\widetilde{\boldsymbol{q}}(r,k) = \int_{-\infty}^{\infty} \boldsymbol{q}(r,z)\exp(-\mathrm{i}kz)\,\mathrm{d}z, \tag{2.7}$$

with $k = k_r + \mathrm{i}k_i$ complex in general. The bulk equations (2.1) and (2.2) subject to regularity conditions at $r = 0$ are formally solved by standard methods (Chandrasekhar 1961) to give for the transformed magnitudes,

$$\widetilde{p}(k,r) = -\mathscr{A}\,\frac{\mathrm{i}(\omega-\beta k)\,I_0(kr)}{k\,I_1(k)}, \tag{2.8}$$

$$\widetilde{u}(k,r) = \mathscr{A}\,\frac{I_1(kr)}{I_1(k)} - \mathscr{B}\,\frac{I_1(k_v r)}{I_1(k_v)}, \tag{2.9}$$

$$\widetilde{w}(k,r) = \mathscr{A}\,\frac{\mathrm{i}\,I_0(kr)}{I_1(k)} - \mathscr{B}\,\frac{\mathrm{i}k_v\,I_0(k_v r)}{k\,I_1(k_v)}, \tag{2.10}$$

where we have used standard notation for the intervening modified Bessel functions. $\mathscr{A}$ and $\mathscr{B}$ are constants to be determined from the remaining boundary conditions. We must also define $k_v^2 \equiv k^2 - \mathrm{i}(\omega-\beta k)/C$, or, by introducing as a new parameter $k_{temp} \equiv \omega/\beta$, we can alternatively write $k_v^2 = k^2 - \mathrm{i}Re(k_{temp} - k)$. The parameter k_{temp} would be the wavenumber (real) in a temporal formulation, which is more meaningful than the frequency itself to determine when the jet is unstable.

Substitution of the solutions (2.8)–(2.10) into (2.3)–(2.5) gives, in matrix form:

$$\begin{pmatrix} -\mathrm{i}(\omega-\beta k) & -1 & 1 \\ -1+k^2 & -\mathrm{i}\dfrac{\omega-\beta k}{k}\dfrac{I_0(k)}{I_1(k)} + 2kC\dfrac{I_1'(k)}{I_1(k)} & -2k_vC\dfrac{I_1'(k_v)}{I_1(k_v)} \\ 0 & 2\mathrm{i}kC & -\mathrm{i}C\dfrac{k_v^2+k^2}{k} \end{pmatrix} \begin{pmatrix} \widetilde{f} \\ \mathscr{A} \\ \mathscr{B} \end{pmatrix} = \begin{pmatrix} 0 \\ \widetilde{T}_n \\ \widetilde{T}_t \end{pmatrix}, \tag{2.11}$$

where primes denote derivatives with respect to the argument and $\widetilde{T}_n$ and $\widetilde{T}_t$ are the transforms of the corresponding stresses. Let $\boldsymbol{L}$ be the 3×3-matrix in (2.11), which has to be inverted to solve the system. Owing to linearity, we can treat the effects of normal and tangential stresses independently by obtaining specific solutions for $\widetilde{T}_t = 0$ and $\widetilde{T}_n = 0$, respectively. Substituting the solution of (2.11) in (2.8)–(2.10), we can express the result as

$$\widetilde{\boldsymbol{q}} = \widetilde{\boldsymbol{q}}_n\widetilde{T}_n + \widetilde{\boldsymbol{q}}_t\widetilde{T}_t, \qquad \begin{pmatrix} \widetilde{\boldsymbol{q}}_n \\ \widetilde{\boldsymbol{q}}_t \end{pmatrix} = \begin{pmatrix} \widetilde{p}_n & \widetilde{u}_n & \widetilde{w}_n & \widetilde{f}_n \\ \widetilde{p}_t & \widetilde{u}_t & \widetilde{w}_t & \widetilde{f}_t \end{pmatrix}, \tag{2.12}$$

with

$$\begin{pmatrix}\widetilde{p}_n\\ \widetilde{p}_t\end{pmatrix} = \begin{pmatrix}\{\boldsymbol{L}^{-1}\}_{22}\\ \{\boldsymbol{L}^{-1}\}_{23}\end{pmatrix} \mathrm{i}(\omega-\beta k)\,\frac{I_0(kr)}{k\,I_1(k)}, \tag{2.13}$$

$$\begin{pmatrix}\widetilde{u}_n\\ \widetilde{u}_t\end{pmatrix} = \left[\begin{pmatrix}\{\boldsymbol{L}^{-1}\}_{22}\\ \{\boldsymbol{L}^{-1}\}_{23}\end{pmatrix}\frac{I_1(kr)}{I_1(k)} + \begin{pmatrix}\{\boldsymbol{L}^{-1}\}_{32}\\ \{\boldsymbol{L}^{-1}\}_{33}\end{pmatrix}\frac{I_1(k_v r)}{I_1(k_v)}\right], \tag{2.14}$$

$$\begin{pmatrix}\widetilde{w}_n\\ \widetilde{w}_t\end{pmatrix} = \left[\begin{pmatrix}\{\boldsymbol{L}^{-1}\}_{22}\\ \{\boldsymbol{L}^{-1}\}_{23}\end{pmatrix}\frac{\mathrm{i}\,I_0(kr)}{I_1(k)} + \begin{pmatrix}\{\boldsymbol{L}^{-1}\}_{32}\\ \{\boldsymbol{L}^{-1}\}_{33}\end{pmatrix}\frac{\mathrm{i}\,k_v I_0(k_v r)}{k\,I_1(k_v)}\right], \tag{2.15}$$

$$\begin{pmatrix}\widetilde{f}_n\\ \widetilde{f}_t\end{pmatrix} = \begin{pmatrix}\{\boldsymbol{L}^{-1}\}_{12}\\ \{\boldsymbol{L}^{-1}\}_{13}\end{pmatrix}, \tag{2.16}$$

where $\{\boldsymbol{L}^{-1}\}_{ij}$ is the ijth element of the inverse of $\boldsymbol{L}$. These elements have a common factor $D(\omega,k)^{-1}$, with $D(\omega,k)=\det(\boldsymbol{L})$. The so-called dispersion relation, $D(\omega,k)=0$ is known to play a fundamental role in the structure of the solution. It is important to realize that the only singularities come from $D(\omega,k)=0$ and not from the remaining parts of these expressions.

By the convolution theorem, it is possible to express the solution in the form

$$\boldsymbol{q}(r,z) = \int_{-\infty}^{\infty} \mathrm{d}z'[\boldsymbol{G}_n(r,z-z')T_n(z') + \boldsymbol{G}_t(r,z-z')T_t(z')] \tag{2.17}$$

where we can identify $\boldsymbol{G}_n$ and $\boldsymbol{G}_t$ as two vector Green functions associated with normal and tangential stresses, respectively:

$$\begin{pmatrix}\boldsymbol{G}_n(r,z)\\ \boldsymbol{G}_t(r,z)\end{pmatrix} = \frac{1}{2\pi}\int_{-\infty}^{\infty}\mathrm{d}k\,\exp(\mathrm{i}kz)\begin{pmatrix}\widetilde{\boldsymbol{q}}_n(r,k)\\ \widetilde{\boldsymbol{q}}_t(r,k)\end{pmatrix}. \tag{2.18}$$

These Green functions are the responses of the system in terms of pressure, radial and axial velocities, and deformation, to spatial δ-Dirac pulses and harmonic time-dependence for the normal and tangential stresses. Although the formulation is better presented simultaneously, as done, it is more clear to study the effect of each stress separately.

2.1. *The inviscid case*

For future reference and owing to its peculiarity in the above formalism, we present here the particular case of inviscid liquids. The limit $C\to 0$ makes the boundary condition for the tangential stress meaningless, i.e. (2.5), in accordance with the mandatory requirement of null imposed tangential stress in a well-posed problem for perfect fluids. We thus omit (2.5), restrict ourselves to an imposed normal stress and set the integration constant $\mathscr{B}$ to zero in the solutions (2.9) and (2.10) and subsequent expressions. Instead of (2.11) we write

$$\begin{pmatrix}-\mathrm{i}(\omega-\beta k) & -1\\ -1+k^2 & -\mathrm{i}\dfrac{\omega-\beta k}{k}\dfrac{I_0(k)}{I_1(k)}\end{pmatrix}\begin{pmatrix}\widetilde{f}_n\\ \mathscr{A}\end{pmatrix} = \begin{pmatrix}0\\ \widetilde{T}_n\end{pmatrix}. \tag{2.19}$$

The transformed magnitudes explicitly become

$$\widetilde{p}_n = \frac{(\omega - \beta k)^2}{D(\omega, k)} \frac{I_0(kr)}{k I_1(k)}, \tag{2.20}$$

$$\widetilde{u}_n = -\frac{\mathrm{i}(\omega - \beta k)}{D(\omega, k)} \frac{I_1(kr)}{I_1(k)}, \tag{2.21}$$

$$\widetilde{w}_n = \frac{(\omega - \beta k)}{D(\omega, k)} \frac{I_0(kr)}{I_1(k)}, \tag{2.22}$$

$$\widetilde{f}_n = \frac{1}{D(\omega, k)}, \tag{2.23}$$

where

$$D(\omega, k) = (\omega - \beta k)^2 \frac{I_0(k)}{k I_1(k)} + (1 - k^2). \tag{2.24}$$

3. Spatial modes

According to the standard analysis of *signalling problems* in open flows (Briggs 1964; Bers 1983; Huerre & Monkewitz 1990), the Green function just determined is the asymptotic or steady-state response of our system to a stimulation defined by a delta spatial distribution and a harmonic temporal dependence. The poles of the Green function are divided in two sets and the Green function itself is constructed for z positive or negative as a sum of the residues at the poles corresponding to each set. Under convective stability conditions, we can consider each term of any of either sums as the contribution of a specific spatial mode of the system. The first characterization of the modes comes from their location in the complex plane and their assignment to the upper or the lower region, according to Briggs' criterion, described in the above references. While the sign of k_r simply determines the phase velocity, the stability depends on both the sign of k_i and the assignment of the pole to the upper or the lower region. We have in principle as many as eight cases describing the direction of phase velocity, growth or decay and positive or negative z (Ashpis & Reshotko 1990).

3.1. *Pole locations*

With all that in mind, in figure 1 we present an example of the distribution of the poles in the complex k-plane, with the indentation of the integration path appropriate to assign them to the correct region: upstream or downstream. We can observe several sets of modes, for which we shall introduce a nomenclature to be explained in § 6.

(*a*) *Capillary modes*. There are two and are located in the upper region of the k-plane ($z > 0$). The sketch of figure 1 shows them for $k_{temp} < 1$ but, as they qualitatively change their location when ω is varied, we also show in figure 2 their branches in the complex k-plane for a significant range of frequencies, along with branches corresponding to other modes. We call them dominant ($\mathrm{C_{dom}}$) and subdominant ($\mathrm{C_{sub}}$) because, in the unstable range, one of them always has a lower value of k_i than the other, the former thus determining the asymptotic behaviour of the jet. The dominant capillary mode is responsible for the capillary instability ($k_i < 0$), occurring for $k_{temp} < 1$, whereas the subdominant capillary mode always decays downstream because $k_i > 0$ (Keller *et al.* 1973; Leib & Goldstein 1986*b*).

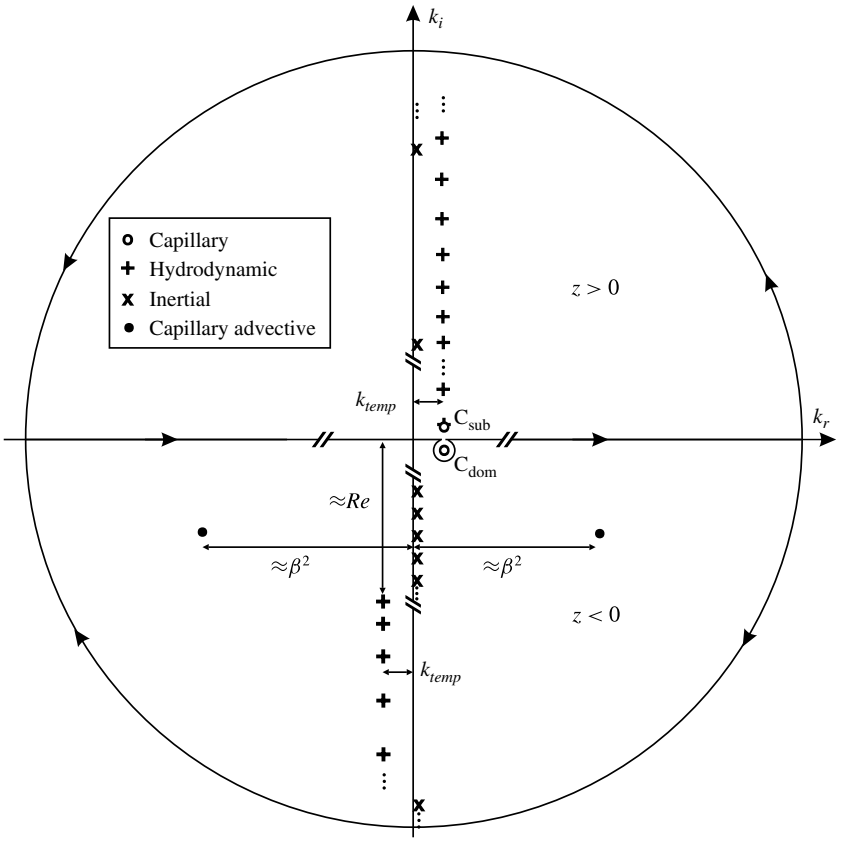

FIGURE 1. Sketch of the poles of the Green functions for values of C and β leading to convective instability, just for a frequency in the unstable range ($k_{temp} < 1$). The upper and lower integration contours respectively enclose the regions labelled $z > 0$ (downstream) and $z < 0$ (upstream, relative to the stimulation point). Symbols used for each family of modes are shown. Rough location indications are also included.

For $k_{temp} > 1$ both of them are either decaying (due to viscosity) or neutral (in the inviscid case). They both propagate downwards and have non-dimensional wavenumbers very close to k_{temp}.

We can estimate their location when $C \ll 1$ and take it as a numerical seed when increasing C up to a prescribed value. To this end, consider the inviscid approximation, as found in Keller *et al.* (1973) in the axisymmetric case, $D(\omega, k) = 0$, with $D(\omega, k)$ given by (2.24). If we assume, for small k, $I_0(k)/I_1(k) \simeq 2/k$, the dispersion relation becomes a quartic equation in this variable. The only two roots consistent with this approximation give the estimates for the capillary modes. The other ones having $|k| > 1$ are discarded.

(*b*) *Capillary advective modes*. There are two, both in the lower region, as shown in figure 1 (thus affecting points with $z < 0$), both decaying but propagating in opposite directions, $\mathrm{CA_{down}}$ downwards ($k_r > 0$) and $\mathrm{CA_{up}}$ upwards ($k_r < 0$), both with small wavelengths, of the order of β^{-2}, as we will see in § 6. The branches obtained by varying the frequency are also shown in figure 2, where we can observe that these poles have opposite real parts and the same imaginary part for

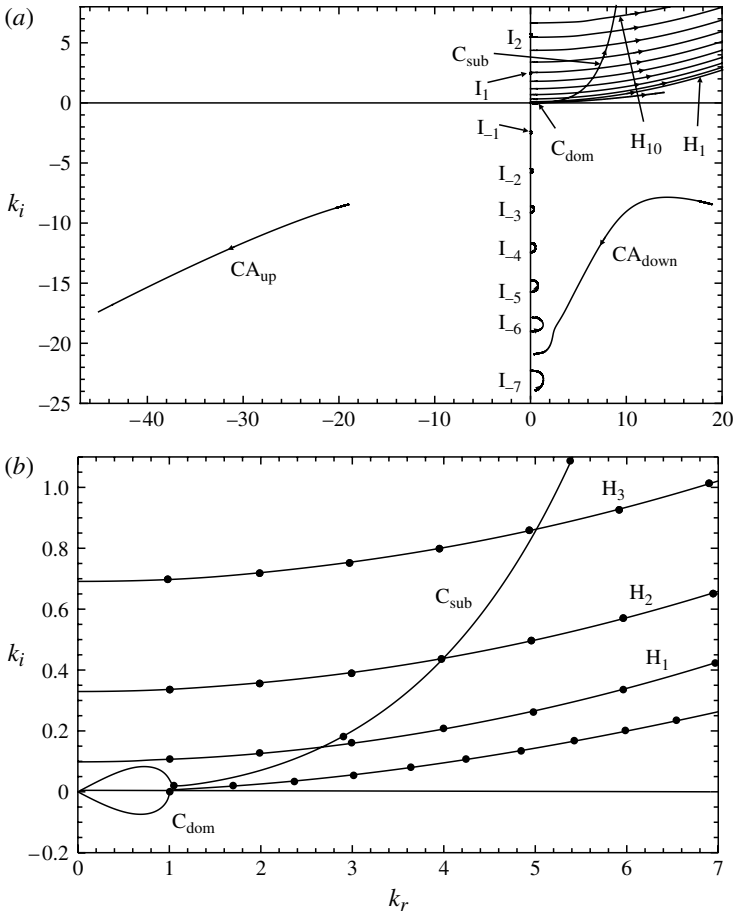

FIGURE 2. (*a*) Spatial branches corresponding to some representative modes, obtained for $\beta = 4.47$, $C = 0.03$ and varying frequency ω. Modes are identified by letters: C_{dom}, dominant capillary; C_{sub}, subdominant capillary; CA_{up}, capillary advective directed upwards; CA_{down}, capillary advective directed downwards; I_i, inertial; H_i, hydrodynamic (indexes in both families indicate order of proximity to the origin, with negative values for modes defined upstream). (*b*) Details of the branches near the origin. On each branch, the circles indicate values of k obtained for integer values of $k_{temp} \equiv \omega/\beta$, starting from 1 on the left, marked to identify corresponding points on different branches. Note that we do not have merging of hydrodynamic and the dominant capillary poles, although the branches intersect.

$\omega = 0$ but have unrelated k for $\omega \neq 0$. The consequences will also be discussed in § 6.

The downward mode was already reported by Busker & Lamers (1989). The upward mode is reported here for the first time. They can be approximately located by considering $|k| \gg 1$ and substituting $I_0(k)/I_1(k) \simeq \mathrm{sgn}(k_r)$ in (2.24). The result is another algebraic equation leading again to two consistent solutions among four.

(*c*) *Inertial modes*. There are two infinite sets of modes, one lying in the upper ($z > 0$) and the other in the lower region ($z < 0$). We denote them by means of the symbols I_i, with positive indexes for the upper region and negative for

the lower one, ordered by distance to the origin. We obtain estimates for $\beta \gg 1$ from the purely imaginary zeros of $I_0(k)$, as seen also from (2.24). Consequently, they represent virtually evanescent modes. The locations of the modes closest to the origin are quite insensitive to variations of any parameter, as illustrated in figure 2(*a*) for varying frequency. This behaviour relaxes as we consider modes of higher order, even leading to eventual degeneracy (only suggested in that figure) between one inertial mode and the capillary advective mode directed downwards.

(*d*) *Hydrodynamic modes*. We find two infinite sets, lying in the upper and lower regions, respectively (see again figure 1). They are shown as H_i, with indexes meaning the same as for the inertial modes. Their real parts are close to $\pm k_{temp}$ (positive for the upper family and negative for the lower one). Their locations are estimated from the zeros of $I_1(k_v)$, because this function appears in the denominator of some of the viscous terms of $D(\omega, k)$, thus producing large variations near these zeros and making possible a balance with the remaining terms in the dispersion relation. As $k_v^2 = k^2 - \mathrm{i}Re(k_{temp} - k)$, by putting $k_v = \mathrm{i}x_{1n}$, with x_{1n} the nth zero of the Bessel function $J_1(x)$, we have two roots, originating the two respective families. For large Re and small or moderate k_{temp}, we find zeros close to $k_n = (k_{temp} + \mathrm{i}x_{1n}^2)/Re$; this implies damped modes propagating in the downward direction and defined for $z > 0$. The estimation for the lower family (defined for $z < 0$) gives an imaginary part approximated by $-Re - x_n^2/Re$, i.e. they are strongly damped for high Reynolds numbers.

Although a rigorous proof of having obtained all the poles of the Green function will not be provided, we have plausible arguments to believe this to be so. For this task, we have made use of the argument principle applied to a rectangular contour to evaluate the number of zeros of an analytic function enclosed in it (Johnson & Tucker 2009). The rectangular geometry facilitates a systematic search by tessellation over a wide domain. The method also gives the location of each zero. Trivial care must be taken to avoid the two branch cuts of $D(\omega, k)$ defined by the condition $k_v = 0$, which are not true branch cuts of the Green functions due to the way in which the variable k_v enters the complete integrands in (2.13)–(2.16). The absence of branch cuts for the definition of the Green function makes the spectrum of spatial modes discrete. This is the usual case when dealing with systems bounded in the spanwise direction (Huerre & Monkewitz 1985).

3.2. *Velocity field*

Once the poles of the Green functions are located, we can complete the characterization of the spatial modes by examining the corresponding velocity fields and surface deformation. The poles are the values $k_j(\omega)$ of the variable k for which the matrix $\boldsymbol{L}$, with coefficients defined in (2.11), is singular. The spatial modes are determined, except for an arbitrary amplitude, from the null space of this matrix, yielding a relation between the integration constants $\mathscr{A}$ and $\mathscr{B}$, and the transform of the deformation, $\widetilde{f}$. We choose a normalization based on the amplitude of deformation for reasons to be discussed later. Assuming $\widetilde{f} = 1$, (2.13)–(2.16) give the functions p, u, w and f with a structure summarized as

$$\boldsymbol{Q}_j(r, z, t) = \mathrm{Re}\{\widetilde{\boldsymbol{q}}_j(k_j, r)\exp[\mathrm{i}(\omega t - k_j(\omega)z)]\}. \tag{3.1}$$

Note that the spatial modes have nothing to do with normal or tangential stresses separately since they are common to both cases.

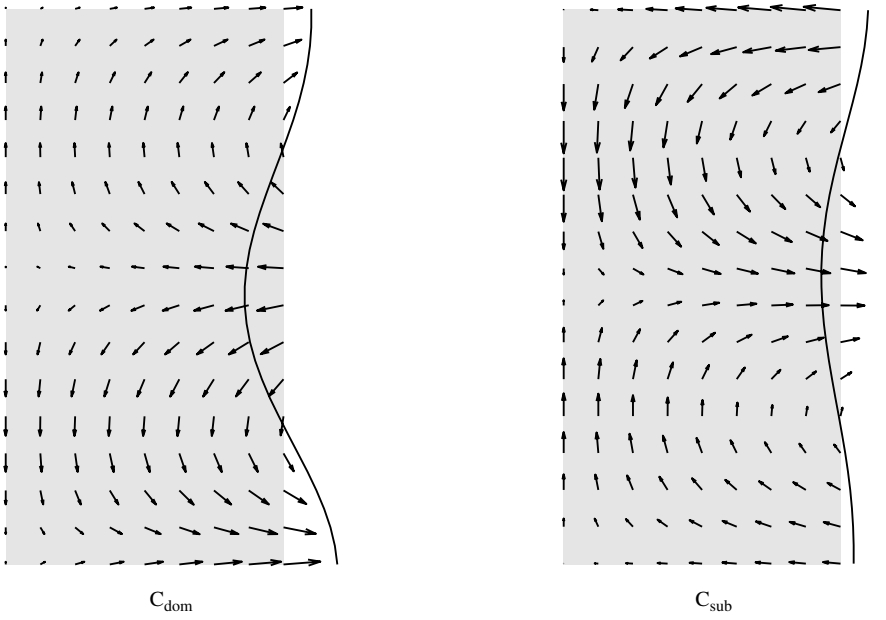

FIGURE 3. Velocity fields for the dominant capillary mode, C_{dom}, and subdominant capillary mode, C_{sub}. The axial coordinate and the axial velocity component are scaled with the wavelength of each mode. The flow goes downwards. Parameters are set to $k_{temp} = 0.7$, $C = 0.03$ and $\beta = 4.47$.

We now describe the salient features of the velocity field associated with each spatial mode.

(*a*) *Capillary modes*. The velocity fields for these two modes are significant over the whole radial profile, have net flow across any section and are clearly associated with the surface deformation. For the dominant mode, f and u are essentially in phase, which implies a net transport of fluid from valleys to crests of the deformation. The opposite occurs for the subdominant mode, which is stable. All these features are apparent in figure 3.

(*b*) *Capillary advective modes*. The velocity field is only significant near the free surface, with strong decay towards the jet axis, as shown in figure 4. There is net flow across any section of the jet. f and u have a phase shift close to $\pi/2$.

(*c*) *Inertial modes*. Modes I_1 and I_2 in figure 5 represent the first two modes of the infinite numerable family in the upper region $z > 0$. The family in the lower region has virtually the same behaviour, so it is not included in the figure. To interpret these figures correctly we must notice that: (i) the free surface and velocity fields are represented without their strong axial decay, which makes these modes virtually evanescent; and (ii) the z coordinate runs over a very long wavelength. Consequently, this figure is most useful as a temporal evolution at a fixed station, rather than a spatial representation, by appealing to the proportionality relation $z = (\omega/k_r)t$ giving constant phase. The movement of the fluid is radially organized in regions with alternating orientation; the number of these regions agrees with the order of the zero of the Bessel function associated with each mode. The radial velocity in the region closer to the free surface is

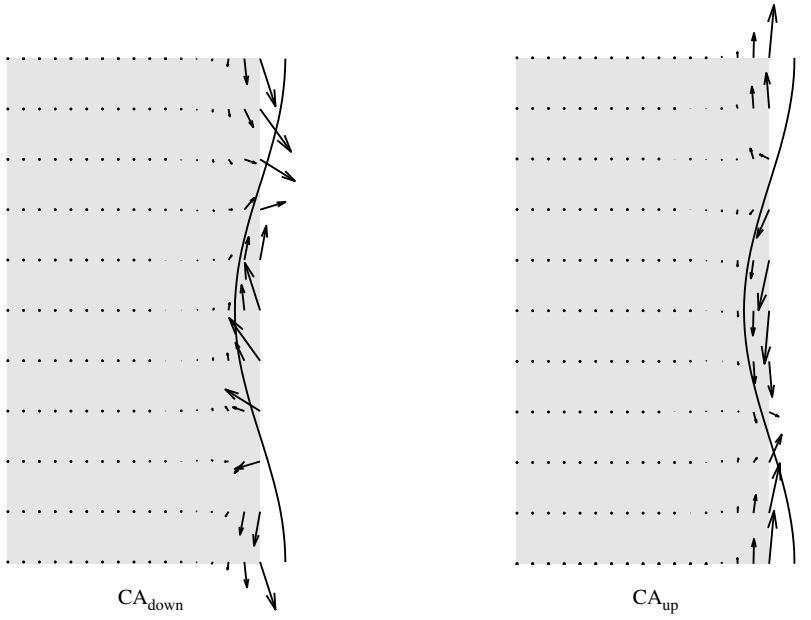

FIGURE 4. Velocity fields for the capillary advective downward mode, CA_{down}, and capillary advective upward mode, CA_{up}. The axial coordinates and the axial velocity components are scaled with the wavelength of each mode. The spatial decay has been omitted by dividing the velocity components by $\exp(-k_i z)$. Parameters are set to the same values as in figure 3.

in phase opposition relative to the surface deformation. There are no recirculating rolls.

(*d*) *Hydrodynamic modes*. We have seen in the previous subsection that two very different families are included in this item. They have in common a non-dimensional wavelength close to $2\pi\beta/\omega$ and a location in the complex k-plane associated with the zeros of $I_1(k_v)$. The modes belonging to the family in the upper region (represented in figure 6) have significant velocity in the whole jet but negligible deformation. The velocity field is radially organized in rolls, and the number of rolls is indicated by the index of the zero with which the mode is associated. The lower family (not represented in the figure) is very strongly damped.

The above description has been limited to unstable jets and particular values of the jet velocity and the Ohnesorge number, but a complete parametric study would necessarily offer a richer behaviour. For instance, for $k_{temp} > 1$ the dominant capillary mode becomes stable. Accordingly, a continuous transition from in-phase to anti-phase between deformation and radial velocity takes place as we increase the forcing frequency beyond the Plateau limit $k_{temp} = 1$. Other changes are also expected whenever large variations in the position in the k-plane take place, including merging of poles. The well-known case leading to absolute instability will be reported in § 5.

4. Application to surface stimulation

A quantitative evaluation of the importance of each mode in the two Green functions is given by the amplitudes which, according to our deformation-based normalization

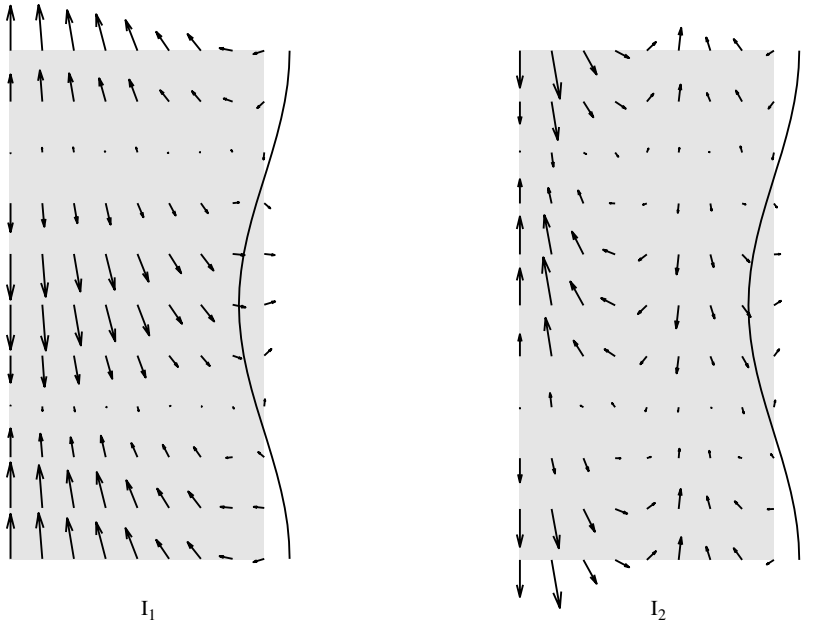

FIGURE 5. Velocity fields for the first two inertial modes defined downstream, I_1 and I_2. The axial coordinates are scaled with their wavelengths, very long. The spatial decay has been omitted by dividing the deformation and the velocity components by $\exp(-k_i z)$. Parameters are set to the same values as in figure 3.

and (2.16), are the residues

$$\begin{pmatrix} f_{n,j} \\ f_{t,j} \end{pmatrix} = \mathrm{Res}_{k \to k_j} \begin{pmatrix} \{\boldsymbol{L}^{-1}\}_{32} \\ \{\boldsymbol{L}^{-1}\}_{33} \end{pmatrix}. \tag{4.1}$$

As an illustration of the relative importance in terms of deformation of each mode for both kinds of stimulation, in table 1 we present the amplitudes obtained through (4.1). Downstream, as a rule, the capillary modes are the most relevant. For the same applied stress, the amplitude is greater for tangential stresses. Concerning the hydrodynamic family, for tangential stresses the first mode has an amplitude of the same order as the capillary modes and as the index of the mode increases the amplitudes decrease. For normal stresses, even the first hydrodynamic mode is negligible with respect to the capillary modes. Although hydrodynamic modes make a modest contribution to the deformation for these particular values of the parameters, we have to keep in mind that their contribution to the velocity field is much greater. Turning now to the inertial family, we find that these modes are more important than hydrodynamic modes for normal stress, while we find the opposite for tangential stress. Upstream, the capillary advective modes take the place of the capillary modes and the hydrodynamic modes are not relevant.

Table 1 can be used to build the Green functions as a sum of spatial modes, each with determined amplitudes and phase shifts relative to the stimulation. However, the number of modes required to give a precise evaluation for a given axial position z increases as z goes to zero. In other words, we have non-uniform convergence. The reader interested in these details, as well as how the superposition of spatial modes

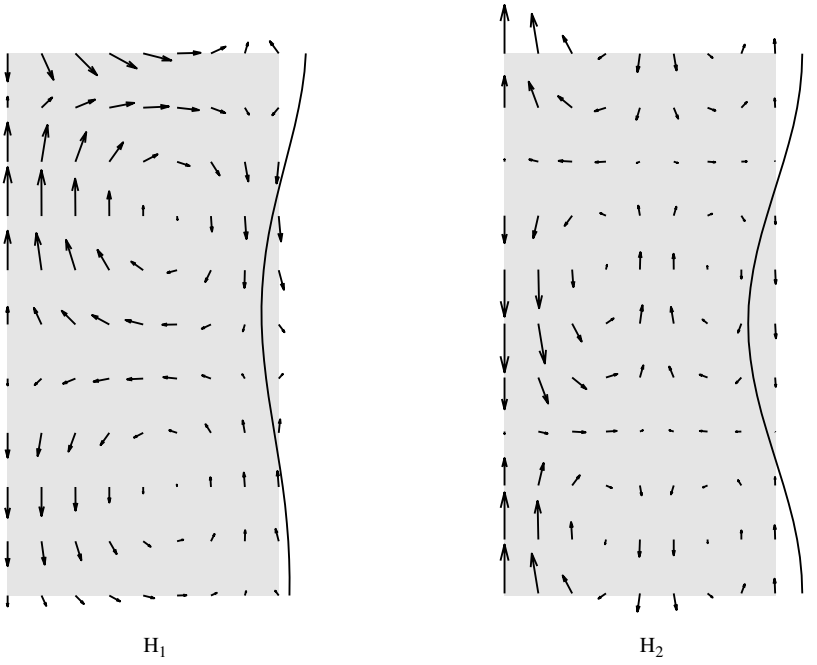

FIGURE 6. Velocity fields for the first two hydrodynamic modes defined downstream, H_1 and H_2. The axial coordinates and the axial velocity components are scaled with the wavelength of each mode. For H_2, the spatial damping is important and it has been omitted by dividing the deformation and the velocity components by $\exp(-k_i z)$. Parameters are set to the same values as in figure 3.

describes the expected downstream relaxation of the radial velocity profile to that of the capillary dominant mode, can consult Guerrero (2011).

We now focus on the amplitude of the dominant capillary mode, f_{Cdom}. Figure 7 shows its modulus as a function of k_{temp} (proportional to the frequency) for fixed jet velocity and various C. The amplitude of the mode typically presents a peak, more or less pronounced, which is located at $k_{temp} = 1$ for an inviscid jet and shifts to greater values as C increases. At the same time, the maximum decreases as C increases. The position and value of the maximum are determined by the minimum distance between the two capillary poles in the k-plane, as we can observe in figure 2(b). In this respect, we recall that we can express the meromorphic function giving the amplitude as a sum of simple fractions with the differences between the dominant capillary pole and all the other poles as denominators (Titchmarsh 1939). In the inviscid case the two poles merge and we find an infinite amplitude. From figure 7 we can conclude that the tangential-stress stimulation is the more efficient one, at least in terms of our stress-amplitude formulation. This is particularly apparent for low frequencies. The cases $\omega \to 0$ give non-zero amplitudes for normal-stress stimulation, but we have checked that the subdominant capillary mode gives just the opposite deformation, thus preventing the unphysical result of a change in radius over the whole jet. For strictly $\omega = 0$ the amplitude is null, in accordance with the degeneracy of the two capillary modes.

If we want to study the effect of the increase of β on the stimulation efficiency, we have to notice that, as we increase the velocity, we diminish the time during which the

Mode	Normal stress		Tangential stress	
	Modulus	Phase	Modulus	Phase
		$z > 0$		
C_{dom}	0.07803	1.38251	0.21565	1.49315
C_{sub}	0.07382	−1.36113	0.14081	−1.59479
H_1	0.00450	−0.73230	0.07557	−1.12441
H_2	0.00003	1.06889	0.00303	−0.23520
H_3	0.00001	3.02601	0.00135	0.74217
I_1	0.01760	−2.03957	0.00574	−1.82033
I_2	0.00700	−1.77400	0.00353	−1.22685
I_3	0.00390	−1.67669	0.00234	−1.11187
		$z < 0$		
CA_{down}	0.05696	0.07403	0.03912	0.67876
CA_{up}	0.04450	−3.14119	0.02994	−0.62410
I_{-1}	0.01975	−1.08667	0.00275	0.20926
I_{-2}	0.00916	−1.38398	0.00104	−0.29875
I_{-3}	0.00560	−1.49103	0.00037	−1.15982
I_{-4}	0.00365	−1.55363	0.00041	−2.44503
I_{-5}	0.00241	−1.59362	0.00057	−2.82490
I_{-6}	0.01584	−1.61838	0.00063	−2.96618

TABLE 1. Modules and phases of the amplitudes of the modes that contribute most in normal- and tangential-stress stimulations. Phases, measured in radians, are relative to the stimulation. The modes are classified according to the region where they are defined. Parameters are set as in figure 3.

stimulation is acting over a fixed wavelength. Therefore, f_{Cdom} is expected to decrease as β increases. This is why in figure 8 we represent the product βf_{Cdom}, which makes more sense than the amplitude alone when varying β. As expected, βf_{Cdom} depends only very weakly on β for k_{temp} far from the peak. Near the peak we observe a monotonic increase of this function, in accordance with a shorter distance between the dominant and subdominant capillary poles. In the limit of infinite jet velocity, the peak becomes infinitely large and narrow.

5. Absolute instability revisited

It is well-known that for each value of the Reynolds number we have a critical value of the Weber number $We_c(Re)$ below which the system becomes absolutely unstable (Leib & Goldstein 1986*b*). The critical curve is reproduced in figure 9(*a*), in terms of our non-dimensional numbers, β and C. Exactly at the critical value, there is marginal absolute instability, characterized by a mode of definite real frequency $\omega_c(C)$ and complex wavenumber $k_c(C)$. These magnitudes are represented in figure 9(*b*). The sketch of figure 1 corresponds to frequencies lower than unity and jet velocities greater than the critical value, i.e. a typical situation manifesting convective instability. The change in the jet velocity would produce a change in the location of the poles. If, for a given C and $\beta > \beta_c(C)$, we select the frequency $\omega_c(C)$, all the poles will be simple, but two of them will tend to merge at the position $k_c(C)$ as $\beta \to \beta_c(C)$. This process, represented in figure 10(*a*), determines which spatial modes are responsible for the absolute instability of capillary jets. We recognize the dominant capillary mode and the capillary advective mode with downward propagation as the merging poles. They

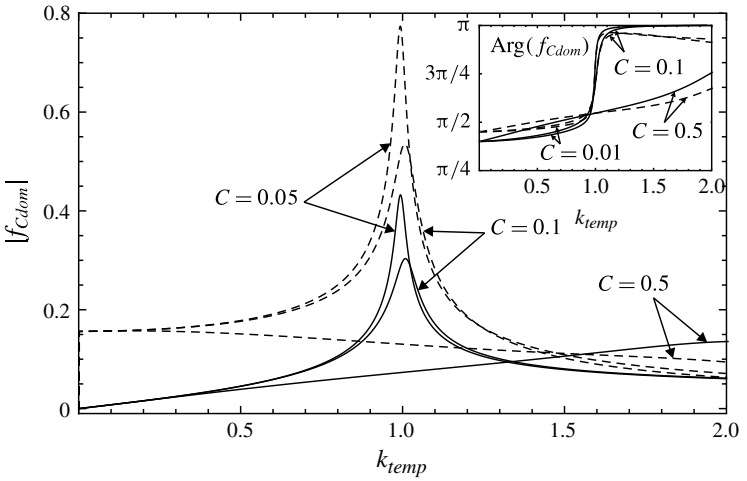

FIGURE 7. Modulus and phase (as an inset) of the amplitude of the dominant capillary mode as a function of $k_{temp} = \omega/\beta$, for normal (solid line) and tangential stresses (dashed line), with jet velocity $\beta = 4.47$ and different values of the Ohnesorge number.

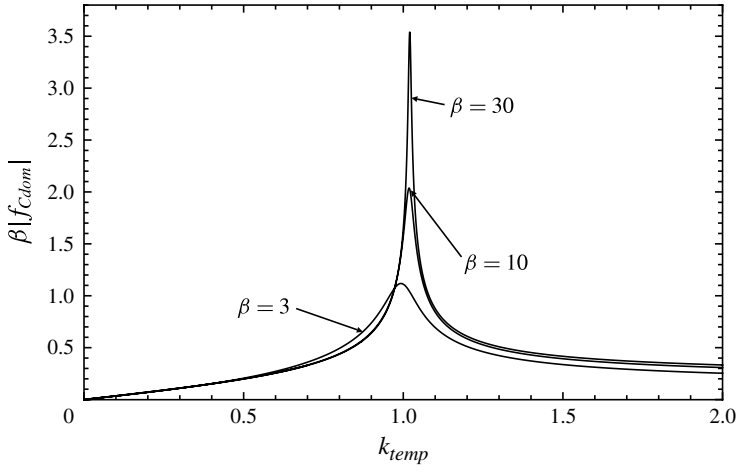

FIGURE 8. Modulus of the product βf_{Cdom} as a function of k_{temp}, for normal stress. The Ohnesorge number is set to $C = 0.1$. Three values of β, 3, 10 and 30, are considered. The factor β in the represented function renders this parametric study more significant.

both have positive phase velocity. The velocity field is the same for both at merging, and is represented in figure 10(*b*). Note that this velocity field differs from those of the dominant capillary and the capillary advective modes represented in figures 3 and 4 respectively: the dominant capillary mode changes the phase shift of the radial velocity relative to the surface deformation, roughly speaking from zero to $\pi/2$, while the capillary advective mode gains in radial extension, now affecting the whole section of the jet. The group velocity of these two modes have opposite signs and tend to zero as their corresponding poles merge.

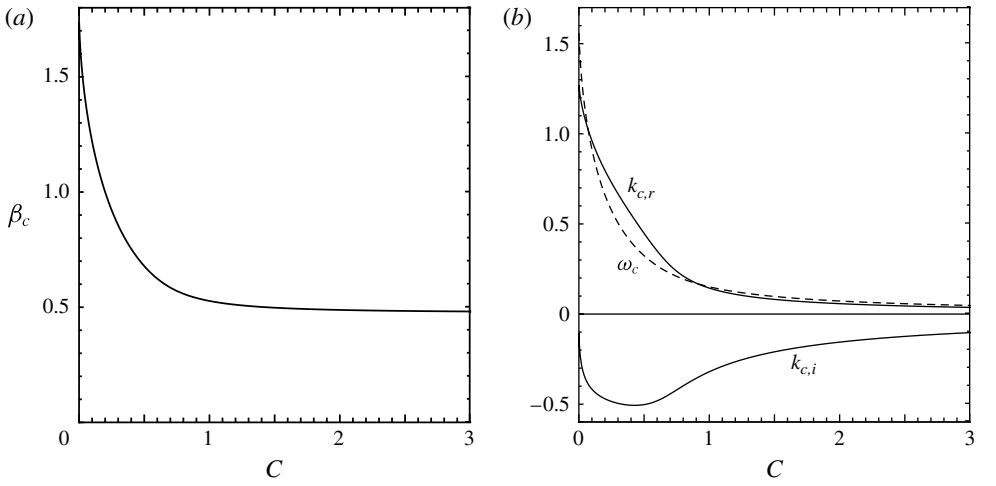

FIGURE 9. (*a*) Curve giving the critical jet velocity as a function of the Ohnesorge number separating the region of convective instability (upper) from that of absolute instability (lower), equivalent to that found by Leib & Goldstein (1986*b*) in terms of Weber and Reynolds numbers. For values exactly on the curve the system has marginal absolute instability. (*b*) Curves of frequency ω_c (real), wavenumber $k_{c,r}$ and the parameter $k_{c,i}$ (spatial growth rate when changed in sign) for neutral absolute instability conditions.

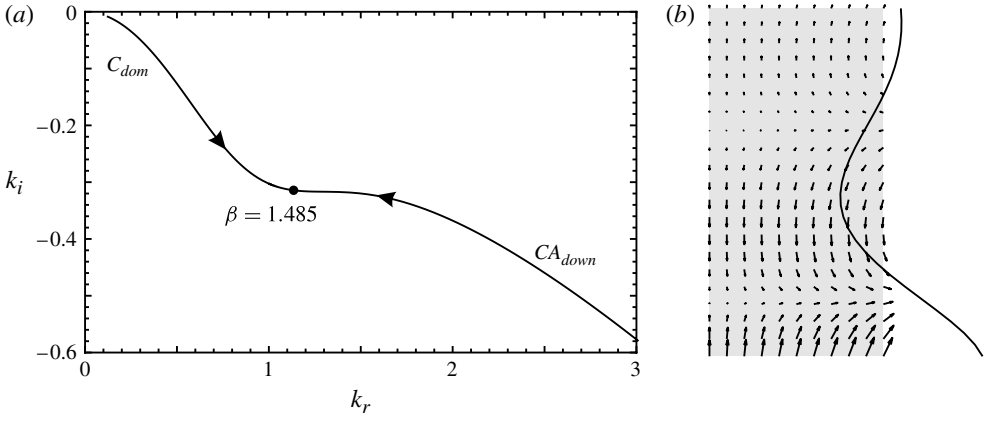

FIGURE 10. (*a*) Merging process of the dominant capillary mode with the downward capillary advective mode as we decrease the jet velocity to its critical value β_c, for a fixed frequency $\omega = \omega_c = 1.2398$ corresponding to the neutral state, and $C = 0.03$. (*b*) Common velocity field for the dominant capillary and the downward capillary advective mode for parameters at the merging point.

6. Discussion

6.1. *Modes*

Although the Green functions obtained in this work are specific to surface stimulation, the spatial modes involved in their construction are universal, in the sense of being potentially present in any other configuration of capillary jets, provided the basic flow

is the same (cylindrical shape and plug velocity profile). It is then expected that if we are interested in a jet issuing from a circular orifice, the problem could be formulated in terms of an appropriate combination of the above-described spatial modes satisfying the conditions at the orifice. This point is relevant to the formulation of boundary conditions for the semi-infinite jet, on which there has been some discussion in the literature (Bogy 1978; Eggers 1997). Criteria for discarding some modes based on their unphysical behaviour are not necessary, once these modes are assigned to the correct region ($z > 0$ or $z < 0$).

The two capillary modes, one of them responsible for the instability of capillary jets, are the best known. Consider first the inviscid case. These two modes are real (purely oscillatory) for $k_{temp} > 1$ and complex conjugate with $k_r \simeq k_{temp}$ for $k_{temp} < 1$ (so one of them growing and the other decaying). The work of Keller *et al.* (1973) states in this case the relation between the temporal and the spatial analysis when the jet velocity is large through an expansion in β^{-1}. Retaining only the first two terms, the two wavenumbers can be expressed (in our non-dimensionalization) as $k_1 \simeq k_{temp} + \omega_R/\beta$ and $k_2 \simeq k_{temp} - \omega_R/\beta$, with $\omega_R(k_{temp})$ the complex frequency given by Rayleigh's temporal analysis of the dispersion relation. In the oscillatory regime they interpreted this as the Doppler shift of two oppositely directed waves when we change to a reference system moving with the velocity of the jet. In the range $k_{temp} < 1$ these same modes are interpreted as purely growing or decaying (according also to Rayleigh's formula) if we change to the system in which the jet is quiescent. Spatial effects other than the bare Doppler shift manifest themselves only for quite small jet velocities because the next terms in the expansions of the two wavenumbers go as β^{-2}. Viscosity does not qualitatively change any of these features. As a conclusion, capillary modes are well understood in the high-jet-velocity limit as a consequence of a Galilean transformation applied to the temporal modes. In this sense, the velocity fields described in figure 3 should be compared with the velocity fields for the temporal modes shown in García & González (2008). However, when we approach absolute instability conditions, significant changes arise, as shown in figure 10(*b*).

The dominant and subdominant capillary modes are not the sole modes having their origin in a balance between capillarity and inertia. Those that we have called capillary advective modes can also be interpreted in this way, although there is an important difference: in the spatial modal analysis we have an additional inertial term due to advection. For the capillary advective modes, the relevant terms in the balance are the capillary forces and the advective inertia, hence the adopted nomenclature. That is why these modes exist even for static forcing ($\omega = 0$). Its advective origin is also the reason for being absent in the temporal analysis. Busker & Lamers (1989) mentioned the existence of a mode additional to those found by Keller *et al.* (1973) and gave his asymptotic expansion in terms of powers of *We* (equivalently β^2 for us). Among the two modes corresponding to both signs,

$$k_{\pm} = \pm\beta^2 + \frac{1}{2} - 2\omega \pm \left(\frac{9}{8} + \omega - 3\omega^2\right)\frac{1}{\beta^2} + O(\beta^{-4}), \tag{6.1}$$

they reported k_+, but failed to discover k_-. Unfortunately, they had a lapsus, as they assigned to k_+ a large wavelength and discarded it as difficult to observe. Also without explicit discussion of its significance, Le Dizès (1997) took into account a third solution of the dispersion relation to construct global modes in falling capillary jets. The additional mode is actually k_+.

Capillary advective modes are nothing other than the well-known capillary waves arising in the interface between two immiscible fluids. Note that these modes typically

have small wavelengths compared to R, since $|k| \sim \beta^2$, so they are essentially the same as in planar geometry. Their velocity field reinforces the analogy, as it is restricted to a depth of the order of the wavelength of the surface perturbations. Pursuing this idea, let us recall that we have in planar geometry a classical problem known as the *fishing line problem*, describing the presence of static capillary waves ahead of an obstacle placed at the surface of a stream (Lamb 1932). Furthermore, anyone can find direct evidence of the existence of similar waves in jets by simply putting a finger under a jet issuing from a tap, in the laminar regime and at low velocity; we can readily observe static corrugations that rise several wavelengths upstream. The same phenomenon has been reported on jets gently entering a horizontal liquid surface (Awati & Howes 1996; Hancock & Bush 2002). These works find qualitative agreement between the measured wavelengths and that arising from a formula that equates the jet velocity to the phase velocity of capillary waves according to Rayleigh's theory. Now we can interpret this formula as the dispersion relation in the inviscid case for spatial modes having $\omega = 0$, and the modes describing this phenomenon as the capillary advective modes. As in the fishing line problem, we have demonstrated that the capillary advective modes exist only in the region upstream the forcing. Having two modes with opposite k_r and equal k_i for $\omega = 0$ allows the construction of static waves of arbitrary initial phase. In this sense, we can clearly see the need for the existence of the pole not reported until now, as we must be able to fit the deformation at $z = 0$ to the requirements of the forcing. On the other hand, no other standing wave is possible for $\omega \neq 0$ in view of the asymmetric location of the poles in this case (see figure 2*a*).

Another important role of the downward capillary advective mode takes place in the origin of the absolute instability, as demonstrated in figure 10. There, we have pursued the intervening modes up to the critical value of the jet velocity, below which we are no longer allowed to call them spatial but instead spatio-temporal modes. Surprisingly, none of the authors who have dealt with absolute instability of capillary jets have clearly identified which spatial modes merge. Leib & Goldstein (1986*b*) just stated the existence of a saddle point of the dispersion relation in the complex k-plane, with zeros originated in opposite half-planes. Yakubenko (1997) associated the structure of iso-lines of complex values of ω' near the merging point in the k-plane with the location of a mode that we now recognize as the first inertial mode, I_{-1}. Finally, Le Dizès (1997), also in the inviscid case, refers to three spatial branches as intervening in the global mode responsible for transition from jetting to dripping. These three branches are the two capillary modes and the downward capillary advective mode. However, as the conclusion of his work is that the transition is governed by a global rather than an absolute instability, he does not discuss the role of these branches in the absolute instability.

The determination of the spatial modes that lead to absolute instability can help to understand the underlying physics. The clues are: (i) the instability can be viewed as a resonance between two modes defined for separate regions, namely, the capillary advective mode in the upstream region and the dominant capillary mode in the downstream region, reaching the same wavelength at criticality; (ii) the merging modes have opposite group velocities leading to evacuation of energy from the stimulation point $z = 0$, but these velocities go to zero at criticality; (iii) it is well-known that an absolute instability is always attached to a distinguished reference: that of the laboratory. In our case, the merging modes are the dominant capillary, unstable in any reference, and one capillary advective, with origin in advection, i.e. genuinely spatial and attached to the laboratory framework.

Let us complete the discussion about the spatial modes by making reference to the remaining, infinite families. Hydrodynamic modes defined for $z > 0$ are understood, like the two capillary modes, in terms of a Galilean transformation of modes existing in the temporal analysis (García & González 2008). That is why $k_r \simeq k_{temp}$ for all of them and their k_i are very close to the damping rate of the temporal hydrodynamic modes divided by β. The reader interested in the detailed description of these modes should consult the above reference. Here we only want to emphasize the three main features of these modes, which are their damping due to viscous dissipation, their negligible associated deformation of the free surface and their recirculating velocity field. Perhaps the most appealing changes when adopting a spatial approach are a non-null mean axial velocity (although still small compared with the recirculation) and the suppression of the interaction described in García & González (2008) between the hydrodynamic family and the subdominant capillary mode. As a final remark, notice that the Reynolds number plays its classical role in determining the typical axial length scale for radial diffusion of axial momentum (Sevilla 2011), being proportional to it. The other hydrodynamic family, defined for $z < 0$, has damping rates k_i at least of the order of the Reynolds number, so their main feature is that they are highly damped.

The remaining modes are the inertial ones, defined both for $z > 0$ and for $z < 0$, which are increasingly decaying as their distance from the origin of the complex k-plane increases. They are evanescent and have a very long wavelength, so we have removed their strong decay from both the velocity field and the deformation, and the z coordinate is normalized with their wavelength to represent them in figure 5; we should emphasize that the figure could be misleading if interpreted as a true spatial picture of these modes. We have adopted the word inertial because capillarity and viscosity do not intervene directly in the location of the poles. In fact, they are even roughly independent of the imposed frequency ω (static modes are possible), as the pole is determined by the geometric condition $I_0(k) = 0$, with a correction of order β^{-2} (Keller *et al.* 1973). As viscosity is not essential for these modes, we can refer to (2.24) in order to understand their origin. There, for the inertial modes, the capillary term is nearly fixed because k does not vary appreciably. Even if we consider a null surface tension (which is equivalent to an infinite value of β) these modes can exist, having zero pressure at the free surface.

As a final remark, we can consider the inertial modes as an illustration of the importance of a stability analysis based on the study of the Green function, rather than directly on the dispersion relation. Indeed, the features of the inertial modes intrigued Keller and co-workers as they did not realize that the family with apparent growing behaviour should be assigned to the upstream region as decaying modes, thus becoming unrelated to the downstream evolution of the jet.

6.2. *Stimulation*

The main result of § 4 is the amplitude of the dominant capillary mode as given by (4.1) for normal- and tangential-stress stimulations. As the jet evolution and breakup is determined by the surface deformation, the best choice for the normalization of modes is that based on the surface deformation. As a counterpart, some modes, like the hydrodynamic modes, have very small associated deformation in relation to the amplitude of the velocity field, so their amplitudes may give a misleading interpretation of their contribution to the whole velocity field. This is not a problem and we simply have to be aware of it. In any case, the velocity field associated with each mode is interesting from a physical interpretation point of view, but not for an evaluation of the ability of a stimulation device to break the jet into drops.

The comparison between amplitudes of the dominant capillary mode for both kinds of stimulation provided by figure 7 is in all cases favourable to the tangential-stress stimulation. It is suggestive to have found the same conclusion as that of the experiments in Barbet (1997) about thermocapillary stimulation, but of course an analysis closer to the experimental conditions is necessary to claim agreement between theory and experiments. In any case, we have already said in § 4 that the superiority apparent in figure 7 cannot be directly interpreted as a higher efficiency of the tangential-stress stimulation in terms of power required for the stimulation.

Results concerning the amplitude of the dominant capillary mode are mathematically understood in terms of distance in the complex k-plane between the pole associated with this mode and the remaining poles, as the residue can be cast as a sum of partial fractions, each inversely proportional to one of these distances. That peak merely reveals the remarkable proximity between the two capillary poles. Consequently, we also have a similar peak for the amplitude of the subdominant capillary mode. In this situation, it is more significant to consider the superposition of both modes. The same applies to the case of imposed frequencies tending to zero.

7. Conclusions

In this work we have carried out a systematic description of the spectrum of spatial axisymmetric modes of the capillary jet. Modes partially described in the literature (like those we have called capillary advective modes), incorrectly interpreted (like the inertial modes) or even fully omitted (hydrodynamic modes), have been taken into account. The description covers aspects like: (*a*) region (upstream or downstream) where the modes are defined; (*b*) propagation and growth features; (*c*) velocity-field features; and (*d*) physical origin. Their relevance has been discussed in relation to several phenomena: static deformation of the jet surface upstream of an obstacle, individual contribution to normal and tangential harmonic surface stimulation (signalling problem) and, finally, the role of some of these modes in the existence of absolute instability. Capillary advective modes are interpreted as the modes in the jet analogous to the capillary waves arising in planar interfaces before an obstacle (fishing line problem). One capillary advective mode is also responsible for the merging with the dominant capillary mode, leading to absolute instability. Results concerning stimulation provide useful information about the linear evolution of the jet subjected to either normal or tangential stresses, through the amplitude of the dominant mode in the Green function.

Acknowledgements

This research was supported by the Spanish Ministerio de Ciencia y Tecnología under contracts FIS2006-03645 and FIS2011-25161, and by the Junta de Andalucía under contract FQM-421.

REFERENCES

ASHPIS, D. E. & RESHOTKO, E. 1990 The vibrating ribbon problem revisited. *J. Fluid Mech.* **213**, 531–547.

AWATI, K. M. & HOWES, T. 1996 Stationary waves on cylindrical fluid jets. *Am. J. Phys.* **64**, 808–811.

BARBET, B. 1997 Stimulations électrohydrodynamique et thermique de jets de liquide conducteur. PhD thesis, Université Joseph Fourier, Grenoble 1, France.

BERS, A. 1983 Space time evolution of plasma instabilities. In *Handbook of Plasma Physics*, pp. 451–517. North Holland.

BOGY, D. B. 1978 Wave propagation and instability of a circular semi-infinite liquid jet harmonically forced at the nozzle. *Trans. ASME: J. Appl. Mech.* **45**, 469–474.

BRIGGS, R. J. 1964 *Electron Stream Interaction with Plasmas*. MIT Press.

BUSKER, D. P. & LAMERS, A. P. G. G. 1989 The nonlinear breakup of an inviscid liquid jet. *Fluid Dyn. Res.* **5**, 159–172.

CHANDRASEKHAR, S. 1961 *Hydrodynamic and Hydromagnetic Stability*. Oxford University Press.

CROWLEY, J. M. 1983 Electrohydrodynamic droplet generators. *J. Electrostat.* **14**, 121–134.

CROWLEY, J. M. 1986 Phased exciter arrays for EHD drop generators. *IEEE Trans. Ind. Applics.* **22** (6), 973–976.

EGGERS, J. 1997 Nonlinear dynamics and breakup of free-surface flows. *Rev. Mod. Phys.* **69** (3), 865–929.

EGGERS, J. & VILLERMAUX, E. 2008 Physics of liquid jets. *Rep. Prog. Phys.* **71**, 1–79.

GARCÍA, F. J. & GONZÁLEZ, H. 2008 Normal-mode linear analysis and initial conditions of capillary jets. *J. Fluid Mech.* **602**, 81–117.

GOEDDE, E. F. & YUEN, M. C. 1970 Experiments on liquid jet instability. *J. Fluid Mech.* **40**, 495–511.

GONZÁLEZ, H. & GARCÍA, F. J. 2009 The measurement of growth rates in capillary jets. *J. Fluid Mech.* **619**, 179–212.

GORDILLO, J. M. & PÉREZ-SABORID, M. 2002 Transient effects in the signaling problem. *Phys. Fluids* **14** (12), 4329–4343.

GORDILLO, J. M. & PÉREZ-SABORID, M. 2005 Aerodynamic effects in the break-up of liquid jets: on the first wind-induced break-up regime. *J. Fluid Mech.* **541**, 1–20.

GUERRERO, J. 2011 Aplicación de campos eléctricos a chorros capilares. PhD thesis, Universidad de Sevilla, Sevilla, Spain.

HANCOCK, M. J. & BUSH, J. W. M. 2002 Fluid pipes. *J. Fluid Mech.* **466**, 285–304.

HUERRE, P. & MONKEWITZ, P. A. 1985 Absolute and convective instabilities in free shear layers. *J. Fluid Mech.* **59**, 151–168.

HUERRE, P. & MONKEWITZ, P. A. 1990 Local and global instabilities in spatially developing flows. *Annu. Rev. Fluid Mech.* **22**, 473–537.

JOHNSON, T. & TUCKER, W. 2009 Enclosing all zeros of an analytic function: a rigourous approach. *J. Comput. Appl. Maths* **228**, 418–423.

KELLER, J. B., RUBINOW, S. I. & TU, Y. O. 1973 Spatial instability of a jet. *Phys. Fluids* **16** (12), 2052–2055.

LAMB, H. 1932 *Hydrodynamics*, 6th edn. Cambridge University Press.

LE DIZÈS, S. 1997 Global modes in falling capillary jets. *Eur. J. Mech. (*B/*Fluids*) **16** (6), 761–778.

LEE, E. R. 2003 *Microdrop Generation*. CRC.

LEIB, S. J. & GOLDSTEIN, M. E. 1986*a* The generation of capillary instabilities on a liquid jet. *J. Fluid Mech.* **168**, 479–500.

LEIB, S. J. & GOLDSTEIN, M. E. 1986*b* Convective and absolute instability of a viscous jet. *Phys. Fluids* **29**, 952–954.

LIN, S. P. 2003 *Breakup of Liquid Sheets and Jets*. Cambridge University Press.

MELCHER, J. R. 1963 *Field-Coupled Surface Waves*. MIT Press.

NAHAS, N. & PANTON, R. 1990 Control of surface tension flows: instability of a liquid jet. *Trans. ASME: J. Fluids Engng* **112**, 296–301.

NICOLÁS, J. A. & VEGA, J. M. 2000 Linear oscillations of axisymmetric viscous liquid bridges. *Z. Angew. Math. Phys.* **51**, 701–731.

PLATEAU, J. 1873 *Statique Expérimentale et Théorique des Liquides Soumis aux Seules Forces Moléculaires*. Gauthier Villars.

RAYLEIGH, LORD 1945 *The Theory of Sound*, 2nd edn, vol. II. Dover.

SEVILLA, A. 2011 The effect of viscous relaxation on the spatiotemporal stability of capillary jets. *J. Fluid Mech.* **684**, 204–226.

SPOHN, A. & ATTEN, P. 1993 EHD multi-electrode stimulation of a conducting capillary jet. *IEEE IAS Annual Meeting*, 1960–1965.

TITCHMARSH, E. C. 1939 *The Theory of Functions*. Oxford University Press.

YAKUBENKO, P. A. 1997 Capillary instability of an ideal jet of large but finite length. *Eur. J. Mech. (*B/*Fluids*) **16** (1), 39–47.